

THE SIGNIFICANCE OF AN INTRINSIC MRI PARAMETER IN THE DIAGNOSIS OF MYOCARDIAL ISCHEMIA

Ph.D. Thesis Summary

Pal Peter Kiss, M.D.

Head of the Doctoral School: Prof. Sámuel Komoly MD, DSc
Head of the Doctoral Program: Prof. Erzsébet Róth MD, DSc
Supervisor: Prof. Tamás Simor MD, PhD

Heart Institute
University of Pécs, Pécs, Hungary

2010

2 INTRODUCTION

2.1 CONTRAST AGENTS AND THEIR IMPORTANCE

MRI signal intensity is principally determined by proton relaxation rates ($1/T_1$ and $1/T_2$). In absence of sufficient contrast between healthy and diseased tissues paramagnetic lanthanide metal ion (usually Gadolinium) containing MRI contrast agents are used. The solubility of free lanthanide aquo-ions at physiological pH is limited. Also, lanthanide aquo-ions are toxic (3), however, organic chelator molecules with negatively charged carboxylate groups can form nontoxic and soluble complexes with Gadolinium. Such complexes are used as MRI contrast agents. Since contrast agents are distributed in body tissue by the blood circulation, differentially between healthy vs. diseased tissue, they can generate relaxation rate differences between the former and the latter, consequently, contrast in MRI images.

2.2 SIGNIFICANCE OF R1 MEASUREMENT

To date, most of the MRI measurements in the clinic have been based on signal intensity (SI) images. In contrast enhanced MRI (ceMRI), the images show tissue differentiation, when they do, on the basis of signal intensity enhancement (SIE). SIE in ceMRI is dependent on contrast agent concentration in the tissue volume element (voxel) represented by the image area in question, but not in a linear fashion. SI is not an intrinsic parameter, rather it is also dependent on the pulse sequence and acquisition parameters used. Another confounding factor is the inhomogeneity caused by the MRI coil, artificially imparting varying SIs to different parts of the prostate depending on their relative position to the coil. The intrinsic physical parameter which is enhanced in linear proportion with contrast agent concentration is the paramagnetic ΔR_1 (longitudinal relaxation rate enhancement), induced by a contrast agent.(4) The R_1 measurement, in the presence of a proper contrast agent, therefore, is not only a quantitative but a reproducible method to detect pathomorphologies.

2.3 CLINICAL APPLICATIONS

Contrast enhanced MRI is an important clinical tool in the management of patients with cardiac diseases. It allows clinicians to assess morphologic and physiologic myocardial characteristics in the same imaging session. Our results suggest that R_1 mapping, eliminating the above detailed factors, may provide quantitative, reproducible information that can be used to follow up patients with myocardial perfusion defects.

It is highly desired to develop a non-invasive diagnostic tool to detect prostate cancer (PC) in its early phase. The presently used diagnostic methods (PSA, needle biopsy, etc) including DCE MRI, can only be used in the developed phase of PC. With our method, in the presence of Gd(ABE-DTTA), it was possible to quantitatively determine the volume of neoplastic mass in the prostate of TRAMP mice in the early, PIN phases.

3 AIMS

3.1 To determine that our contrast agent Gd(ABE-DTTA) has a signal enhancement capability in the entire magnetic field range we are planning to carry out our experiments

3.2 To determine whether R1 mapping method is capable to provide more information than signal intensity MRI images. To investigate this question we will use R1 mapping in a canine ischemia-reperfusion model. Addition to that, R1 mapping will be carried out in a pixel-by-pixel manner, providing the highest possible resolution of the actual MRI instrument used in the experiment.

3.3 To determine whether R1 mapping can provide detailed information similarly to the myocardial ischemia model, in more than one pathomorphologies, namely, in a mouse model of the prostatic neoplasia.

4 THE UNIQUE R1 CHARACTERISTICS OF Gd(ABE-DTTA)

4.1 INTRODUCTION

The agent Gd-ABE-DTTA (Fig1) has been developed in our laboratory (5).

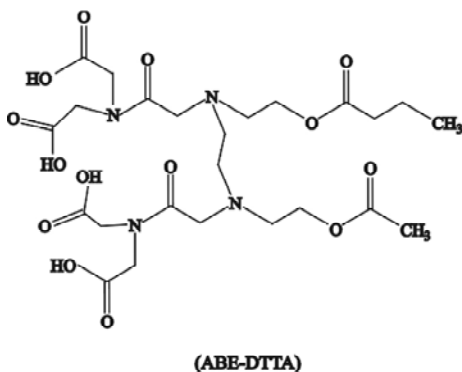


Figure 1. The molecular scheme of the (ABE-DTTA) ligand.

We successfully have used it to detect ischemic defects in the myocardium (5,6). In recent studies, we have also used it to detect myocardial infarction (7). It has shown no deleterious physiological effects at the level of the MRI-effective dose in the canine model (8). The magnetic field dependence of the longitudinal relaxivity of this agent, particularly at high and very high fields (3-14 T) showed unique characteristics.

4.2 MATERIALS and METHODS

Gd(ABE-DTTA) was synthesized, and sample preparation was carried out, as described by Saab-Ismail et al [15]. Proper samples of a concentration of 0.5mM were prepared for NMR and MRI instruments.

All measurements were carried out on 20 C°. In the range 0.0002-1.0T, the field dependence of the longitudinal relaxivity of Gd(ABE-DTTA) was assessed with NMRD as detailed by Koenig and Brown [18]. At field strengths above 1T a variety of single-field MRI and NMR instruments were used. In the experiments using an NMR spectrometer the R1 values were calculated from the signal intensities by the WINNMR software running on the individual NMR instrument using the Equation 1.

$$I_{(t)} = I_{(0)} + A \cdot \exp(-\tau/T_1) \quad (1)$$

where $I_{(t)}$ is the measured intensity and τ is the interpulse delay time. $I_{(0)}$, A and T_1 were the variable parameters of the three parameter curve fitting.

In the experiments carried out on MRI instruments, the images, acquired with different TIs, were exported to a PC computer as image stacks.

From signal intensity changes, the relaxation rate enhancement, ΔR_1 , induced by the contrast agent, was obtained from

$$\Delta R_1 = 1/T_{1(\text{obs})} - 1/T_{1(\text{o})} \quad (2)$$

where $T_{1(\text{obs})}$ was the observed water proton relaxation time in a solution with the contrast agent, and $T_{1(\text{o})}$ was the relaxation time of pure water. In turn, the relaxivity r_1 was calculated from

$$r_1 = \Delta R_1 / c \quad (3)$$

where c was the concentration (in mM) of the contrast agent.

4.3 RESULTS

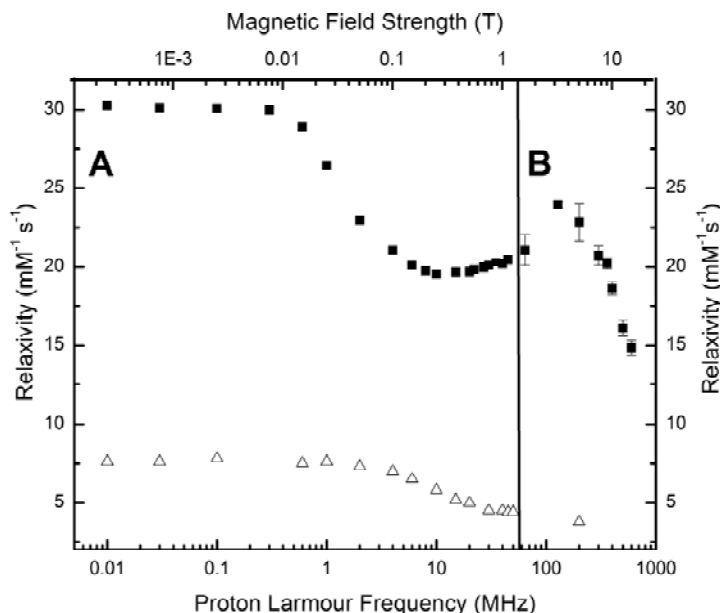


Figure 2 Field Dependency Profile of the longitudinal relaxivity of Gd(DTPA) and Gd(ABE-DTTA) **Figure 2 (A)** The relaxivities (■) of 0.5 mM aqueous solutions of Gd(ABE-DTTA) and of Gd(DTPA) (Δ) acquired with NMRD as a function of magnetic field strength. The Gd(DTPA) NMRD data were adapted from Kellar et al. (70). The measurements of Gd(ABE-DTTA) were carried out at 20 °C whereas the measurements of Gd(DTPA) were carried out at 25 °C. **Figure 2 (B)** The relaxivity at 20 °C of Gd(ABE-DTTA) (■) (n=12) and Gd(DTPA) carried out on a series of single field MRI and NMR instruments detailed in Table 1 as a function of magnetic field strength. The 4.7T datapoint for Gd(DTPA) (Δ), was adapted from Mikawa et al. (71). This study was carried out at 25 °C.

In Figure 2, relaxivity values measured on the NMRD machine (Fig. 2A) and seven different single-field instruments (Fig. 2B) are plotted as a function of magnetic field strength. Similarly to other contrast agents, GD(ABE-DTTA) (molecular weight=760) shows its maximum relaxivity at magnetic field strengths less than 0.01 T, with a high

relaxivity value, above $30 \text{ s}^{-1}\text{mM}^{-1}$, unusual for a small molecular weight agent, and which is only found with macromolecular complexes.

Its relaxivity reaches a local minimum ($\sim 19 \text{ s}^{-1}\text{mM}^{-1}$) around 0.2-0.3 T (Fig. 2A). In distinction from the typical agents presently used in the clinic, its relaxivity increases with field strength above this point, reaches a local maximum around 5T (Fig 2B), and starts decreasing. Nevertheless, even at 8.5 T it is not lower than its relaxivity at 1.5 T.

At the most widespread magnetic field presently used in clinical practice, 1.5 T, the relaxivity was $21.5 \text{ s}^{-1}\text{mM}^{-1}$, a value considerably larger than that of presently used contrast agents. As the field increases, the relaxivity of Gd(ABE-DTTA) further increases, reaching a peak of almost $24 \text{ s}^{-1}\text{mM}^{-1}$ in the vicinity of 3T. It is noteworthy that even around 10T, the relaxivity is still at the considerably high level of $18.5 \text{ s}^{-1}\text{mM}^{-1}$.

4.4 CONCLUSIONS

We suggest that the chemical structure of the ABE-DTTA ligand (Fig. 1), with its lipophylic butyryl chain, may provide the explanation. Such lipophylic chains may lead to micelle formation, increasing the effective radius of the aggregate complex, and leading to the observed field dependency profile. Irrespective of the exact mechanism of its relaxivity, considering the historic trend of the development of clinical MRI instruments that operate at increasingly higher magnetic fields, Gd(ABE-DTTA) could become the contrast agent of choice in cases where high field imaging would be particularly useful.

5 IN VIVO R1-ENHANCEMENT MAPPING OF CANINE MYOCARDIUM USING CEMRI WITH Gd(ABE-DTTA) IN AN ACUTE ISCHEMIA-REPERFUSION MODEL.

5.1 INTRODUCTION

A non-invasive imaging method to visualize acute myocardial ischemia is highly desirable. Contrast-enhanced MRI (ceMRI) can visualize myocardial ischemia with less risk, but the present techniques of cardiac ceMRI could be improved on in the area of spatial resolution and coverage. In this work we present results obtained by R1 mapping, which in conjunction with a long tissue-lifetime contrast agent (CA), Gd(ABE-DTTA), provides quantitative pixel-by-pixel information on myocardial underperfusion.

For reasons detailed in INTRODUCTION, a three dimensional (3D) ΔR_1 map of the heart in ceMRI is a faithful representation of CA distribution with a spatial resolution down to the voxel-by-voxel level.

Unfortunately, however, with MRI instruments presently used in the clinic, the acquisition of images using inversion recovery (IR) for a typical R1 map currently requires 15 minutes of scanning time per tomographic slice. Thus, the myocardial lifetime of CAs presently used in the clinic is too short for obtaining a R1 map of the left ventricle (LV) with IR. To solve this problem, we have introduced an agent that remains in tissue long enough to allow the generation of a R1 map.

5.2 MATERIALS and METHODS

Canine Preparation

Eleven male mongrel dogs weighing 17-19 kg were used in our study. An open-chest non-survival ischemia-reperfusion model was used in our experiments. After a left side thoracotomy, a 1 cm long section of the left ascending coronary artery (LAD) was isolated from its bed. A silk tie was placed around the LAD to allow occlusion during the ischemia.

Experimental Protocol

In Figure 3 the time line of our experimental protocol is illustrated (Fig.3).

	CONTROL	ISCHEMIA	REPERFUSION
Treatment	Normal flow in LAD Blue microspheres administered	Zero flow in LAD 5 th minute: Lemon microspheres administered	Post-ischemic flow in LAD 5 th minute: Eosin microspheres administered
Duration	40 min	30 min	40 min
MRI Sequences	Long and short axis cine images and IR images w/ various TIs acquired	From 10 th to 30 th minutes: Long and short axis cine images and IR images w/ various TIs acquired	From 10 th to 40 th minutes: Long and short axis cine images and IR images w/ various TIs acquired

Figure 3 Timeline of the experimental protocol. Left anterior descending coronary artery: LAD, inversion recovery (IR), inversion time (TI).

At the end of the reperfusion period the animal was euthanized.

Analysis of Microsphere Perfusion

The tissue and blood samples was carried out as described by Simor et al (38) to calculate myocardial perfusion determined by colored microspheres (MP).

Contrast Agent

Contrast agent was prepared and relaxivity was tested as detailed above.

MRI

Slice Orientations

A 7 slice short axis image grid was positioned on the end diastolic image of a four chamber long axis cine image set with a slice thickness with what the grid would cover the entire left ventricle. Since the duration of the 30 minute ischemia was insufficient to cover the entire LV, only one ischemic slice was chosen to determine R1. Cine MRI (using an SSFP sequence), however, was acquired covering the entire LV to determine myocardial function.

Normalized $\Delta R1$ mapping

An IR prepared segmented fast gradient echo sequence was used on a 1.5 Tesla GE Signa Horizon CV instrument to determine R1. The R1 values for each region of interest (ROI) were calculated by curve fitting from the TI-dependent signal intensities using Equation :

$$SI = SI_0 (1 - A \cdot e^{-TI \cdot R1} + e^{-TR \cdot R1}) \quad (Eq 2)$$

Where SI stands for observed signal intensity, SI_0 for signal intensity at equilibrium, TI for inversion time, TR for repetition time, and A is a parameter ($A \leq 2$) obtained by the curve fitting procedure. The rightmost exponential term corrects for signal saturation.

Two alternative post-acquisition calculations with two different spacial resolutions were both carried out: a) R1 values were calculated for each myocardial sector serving as ROI according to the physical sectors in which myocardial perfusion was determined using microspheres; and b) R1 values were also calculated with a voxel-by-voxel resolution (each voxel as an ROI) exploiting the maximum spatial resolution potential provided by the equipment and the imaging pulse sequence.

Image Analysis

MR Analytical Software System (MASS) Version 5.0 (Medis, Leiden, Netherlands) was used for image analysis. The corresponding signal intensity values of a set of IR images with varying TIs were used to determine R1 values of the myocardial ROIs. Myocardial function was determined using data calculated from SSFP movies.

Function and $\Delta R1$ Data Analysis:

Signal intensity (SI) data for each ROI were also measured. MRI SI along with cardiac function data, such as wall thickening (WT); and wall motion (WM) data were derived from the same myocardial volume elements. Corresponding data tables of WT and SI were then generated for the entire image set and processed. An R1 value was calculated for each individual ROI, thus generating an R1 map. An R1 enhancement ($\Delta R1_{ca}$) as defined by Eq 3, induced by CA in a given pixel, is proportional to the concentration of the CA in the voxel represented by that pixel.

$$\Delta R1_{ca} \sim R1_0 \cdot [CA] \quad (\text{Eq 3})$$

Where $R1_0$ is the precontrast R1. This concentration is perfusion dependent, and thus the $\Delta R1$ value of a given pixel is proportional to the perfusion in its voxel. The observed relaxation rate ($R1_{obs}$) of a given pixel in the presence of the CA is the sum of the control relaxation rate $R1_0$ obtained in the absence of the CA and the relaxation rate enhancement $\Delta R1_{ca}$ induced by the CA. Therefore,

$$\Delta R1_{ca} = R1_{obs} - R1_0 \quad (\text{Eq 4})$$

In comparison with corresponding MP values, sectors with $\Delta R1$ less than or equal to 0.8 s^{-1} were considered representing ischemic ROIs ($\Delta R1_{cai}$). Thus, sectors with $\Delta R1$ values larger than 0.8 s^{-1} represented non-ischemic, remote sectors ($\Delta R1_{car}$).

To eliminate differences in R1 data among the individual dogs due to potential differences in effective contrast agent tissue uptake, all $\Delta R1$ values were normalized to the average of the $\Delta R1$ values observed in the non-ischemic areas ($\Delta R1_{car}$) in each individual dog.

$$\Delta R1_n = \Delta R1_{cai} / [\Delta R1_{car}] \quad (\text{Eq 5})$$

The calculated values were compiled as a function of anatomical position. These normalized $\Delta R1_n$ data from all ROIs in a given dog constitute the R1-enhancement map ($\Delta R1_n$) which represents the myocardial perfusion distribution.

Regional Function Analysis:

A regional function map corresponding to the $\Delta R1_n$ map was generated. Myocardial function of each individual sector was also compared to the corresponding myocardial perfusion and $\Delta R1_n$ data.

Pixel-by-pixel Image Analysis:

To determine the $\Delta R1_n$ values in the myocardium with a higher spatial resolution, a series of eight superimposable 60 pixel by 60 pixel image sections, containing the LV, was selected from the MRI images acquired with the eight different TIs. An automated algorithm was applied to determine the R1 value in each voxel associated with each pixel, using Equation 2.

Perfusion Map:

The relaxation rate, consequently the $\Delta R1_n$, of a given pixel is proportional to the concentration of the CA. This concentration is perfusion dependent, and thus the $\Delta R1_n$ value of a given pixel is proportional to the perfusion. Based on this correlation, the pixel-by-pixel $\Delta R1_n$ map can be transformed into a pixel-by-pixel perfusion map (PM).

Percent Perfusion Map (PPM):

To establish a scale to convert $\Delta R1_n$ values to perfusion values, the pixel with the maximum $\Delta R1_n$ value ($\Delta R1_{nmax}$) in that myocardium is sought. To calculate the exact percent perfusion value in each individual voxel, the following derivation applies:

$$\begin{aligned} \Delta R1_{nmax} &\sim \text{Perfusion}_{max} \\ \Delta R1_{nmin} &\sim \text{Perfusion}_{min} \end{aligned} \quad (\text{Eq 6})$$

$$\Delta R1_n \sim \text{Perfusion}$$

$$\Delta R1_n / \Delta R1_{nmax} = \text{Perfusion} / \text{Perfusion}_{max}$$

$$\text{Perfusion} = (\Delta R1_n / \Delta R1_{nmax}) \cdot \text{Perfusion}_{max} \quad (\text{Eq 7})$$

Thus, to express the perfusion in any given voxel as a percent of the maximum perfusion in a particular LV, a Percent Perfusion (PP) parameter is calculated from Eq 5:

$$\text{PP} = (\Delta R1_n / \Delta R1_{nmax}) \cdot 100 \quad (\text{Eq 8})$$

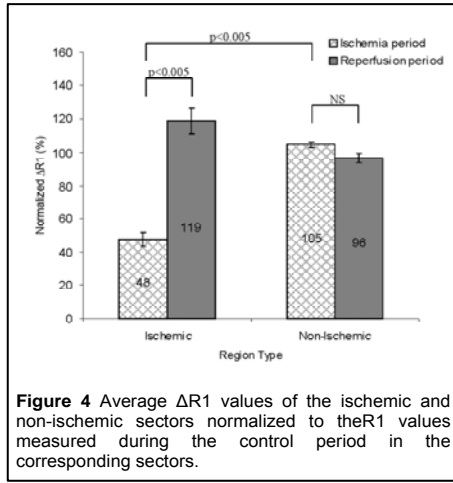


Figure 4 Average $\Delta R1$ values of the ischemic and non-ischemic sectors normalized to the $R1$ values measured during the control period in the corresponding sectors.

test ($p < 0.001$). Upon reperfusion, the difference not only decreased, but due to likely hyperemia and a consequently higher CA concentration in the previously ischemic myocardium, the $\Delta R1_n$ value increased in these areas compared to the non-ischemic areas. This difference, however, was not significant. In Figure 6 the $\Delta R1_n$, WT and WM maps of the same single tomographic slice from one of the dogs are shown along with the corresponding MP.

The matrix containing the PP values of all voxels then yields the Percent Perfusion Map (PPM).

5.3 RESULTS

In Figure 4 are depicted the mean \pm standard error of $\Delta R1_n$ values calculated in ischemic ($n=47$) and non-ischemic sectors ($n=94$) of the eleven dogs. Using normalized $\Delta R1$ values (see METHODS section) all the $\Delta R1_n$ values obtained in the 11 dogs were made animal-independent and thus comparable.

Following CA administration, during the ischemia period a significant $\Delta R1_n$ difference was found between the ischemic and non-ischemic ROIs by using Mann-Whitney Rank

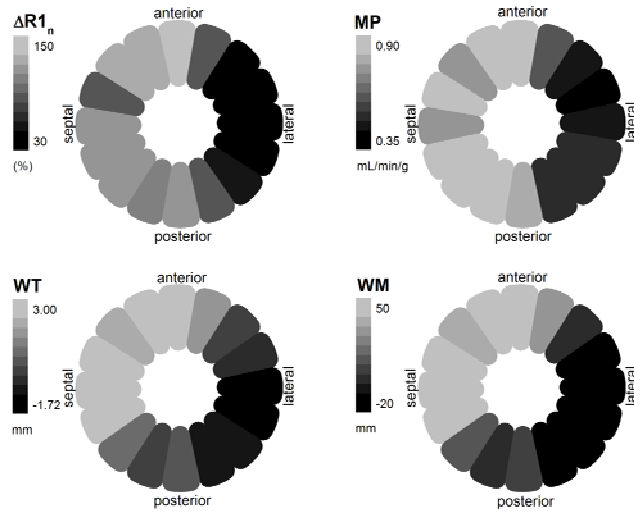


Figure 6 Each rosette illustrates one of the maps: $\Delta R1_n$, MP, WT, and WM, as a function of the position of a given myocardial sector. Similar colors for all parameters were applied to emphasize the correspondence among the parameters.

Mann-Whitney Rank test was used to determine the displayed p values of this comparison. To illustrate the correspondence among the $\Delta R1_n$ map, myocardial perfusion, and the two myocardial function maps, similar colors were used for all four parameters (Fig.6). Pairwise correlations were determined between $\Delta R1_n$ and WT, $\Delta R1_n$ and WM, and $\Delta R1_n$ and MP in all ischemic sectors evaluated in eleven dogs using Pearson's Product Moment Correlation. The

correlation coefficients are compiled in Table 3.

Parameters	Correlation coefficient (<i>R</i>)	p value
$\Delta R1_n$ vs. MP	0.694	P<0.005
$\Delta R1_n$ vs. WT	0.534	P<0.005
$\Delta R1_n$ vs. WM	0.529	P<0.005

5.4 CONCLUSIONS

The present study demonstrates the usefulness of normalized $\Delta R1$ mapping using Gd(ABE-DTTA) for measuring myocardial perfusion and thus quantitatively delineating the ischemic regions *in vivo*. The $\Delta R1_n$ map reflects the distribution of the CA concentration in the myocardium, and thus it is able not only to visualize, but also to quantify, the extent of ischemia in the myocardium. $\Delta R1_n$ mapping visualizes R1 increases induced by a CA more effectively than the usual T1-weighted signal intensity images. Such mapping, however, requires a contrast agent with a myocardial life-time long enough to allow the relatively long acquisitions needed for accurate determination of R1. Gd(ABE-DTTA) is a contrast agent whose sufficiently long myocardial lifetime maintains agent concentration practically unchanged in the course of a complete set of R1 acquisition.

6. USING THE SAME METHOD IN A DIFFERENT DISEASE: VIRTUAL *in vivo* BIOPSY MAP OF EARLY PROSTATE NEOPLASM IN TRAMP MICE

6.1 INTRODUCTION

Prostate Intraepithelial Neoplasia (PIN) is precancerous neoplasia of the prostate and most patients with PIN will develop carcinoma within 10 year. A noninvasive method, like MRI, for the detection of such an early marker would be highly desirable. Our results indicate that the contrast agent Gd(ABE-DTTA) is distributed in the prostate in the TRAMP mouse model in inverse proportion to the tissue's neoplastic content. We wish to suggest such a method, ceMRI combined with our contrast agent, Gd(ABE-DTTA), using a particularly useful method of image analysis, R1 mapping. In our study in twelve TRAMP and three control mice, we have shown that prostate tissue with early high-grade PIN and/or still well-differentiated adenocarcinoma (WD) can be distinguished by our method from normal tissue and/or low-grade PIN.

6.2 METHODS

Contrast Agent (Gd(ABE-DTTA))

The contrast agent Gd(ABE-DTTA) was synthesized and sample preparation was carried out as described above on page 19.

Anesthesia and Contrast Agent Administration Prior to MRI Sessions

Mice were initially anesthetized using 0.15 vol% Isoflurane and was reduced to 0.12 vol%. The tail vein was punctured and Gd(ABE-DTTA) was administered at a dose of 0.05 μmol per gram body weight. The mouse then was placed in the MRI coil.

MRI

A 4.7T Bruker MRI scanner was used, equipped with a 78 mm diameter body coil. Following the initial setup (tuning, shimming, receiver gain setting, etc.), a quick T2-weighted image set was acquired to determine the position of the prostate. Once done, a single 2 mm thick tomographic slice, containing the entire organ and typically close to the coronal orientation with the urethra in the center, was oriented through the prostate. This slice was used to acquire the R1 map for of the prostate using an inversion recovery (IR) sequence with the following parameters: FOV: 5 cm, matrix: 128·128, voxel size: 0.39mm·0.39mm·2mm, number of slices: 1, recycle time (TR): 3000 ms, inversion times (TI): 60, 100, 200, 300, 600, 800, and 1000 ms. At the end of the MRI session the mouse, still anesthetized, was euthanized using a mixture of ketamine and xylazine overdose followed by cervical dislocation.

R1 map:

The part of the image that contains both lobes of the prostate was selected as region of interest (ROI) for analysis. The R1 value of each pixel in the 60x60 pixel matrix was calculated from the SI vs. TI dependence, similarly as it was explained above.

Normalized R1 Map and Neoplastic Index Map

To eliminate possible differences among animals, the R1 values measured in a prostate region have been normalized to the R1 value measured in the thigh muscle ($R1_{norm}$) of the same animal. Following the administration of the contrast agent, we have observed that voxels with the lowest relaxivity ($R1_{lo}$) in a given prostate correspond with prostate

regions that contain the largest amount of tissue that has histology scores 3-4 (see METHODS section). Conversely, voxels with the highest relaxivity ($R1_{hi}$) have been those that contain the least amount of tissue with scores 3-4. The relaxivity of any given voxel is thus governed by the relative proportions of tissue with scores 1-2 versus tissue with scores 3-4. Therefore the R1 value ($R1_v$) measured in any given voxel (v) in the prostate will be found on an R1 scale that ranges between $R1_{hi}$ and $R1_{lo}$. Thus the difference $\Delta_v = R1_{hi} - R1_v$ reflects the extent of neoplasticity in that voxel. When $R1_v = R1_{hi}$, Δ_v is zero, indicating no neoplasticity. When $R1_v = R1_{lo}$, Δ_v obtains its maximum value, reflecting a fully neoplastic voxel. A percent neoplastic index (NI_v) can be then calculated in every voxel v by normalizing Δ_v with the maximum range; i.e. $R1_{hi} - R1_{lo}$ (Eq 2).

$$NI_v = \frac{\Delta_v \cdot 100}{R1_{hi} - R1_{lo}} \quad \text{Eq 2}$$

NI_v will take the value of 100% when $R1_v = R1_{lo}$ (maximum neoplasticity) and zero when $R1_v = R1_{hi}$ (fully normal tissue). Thus, by calculating the NI_v value for all voxels, the pixel-by-pixel R1 map of the prostate can be converted into a voxel-by-voxel NI map reflecting quantitatively the neoplastic content of every given voxel in the map.

Based on the NI_v value of all prostate voxels in a given prostate, the total volume of the cells with score ≥ 3 (Neoplastic Volume, NV) can be calculated from Equation 3:

$$NV = V_v \cdot \sum_{v=1}^n NI_v \quad [\text{Eq 3}]$$

Where V_v is the voxel volume and n is the number of prostate voxels.

The NV values obtained from our experiments are compiled in Table 4.

Table 4. Total prostate volume, mean NI ($\overline{NI_v}$), NI border values, neoplastic volume values, acquired in the twelve TRAMP mice, are shown. The lowest NI values acquired in a region with a histological score 3 or above were considered NI border values.

	Prostate Volume (μL)	NI Border Value		Neoplastic Volume (μL)
TRAMP 1	266	0.68	64	181
TRAMP 2	120	0.70	69	84
TRAMP 3	84	0.77	70	64
TRAMP 4	80	0.75	64	60
TRAMP 5	91	0.62	69	57
TRAMP 6	313	0.68	68	213
TRAMP 7	216	0.71	76	153
TRAMP 8	275	0.57	62	157
TRAMP 9	145	0.61	65	88
TRAMP 10	124	0.71	61	88
TRAMP 11	413	0.62	62	256
TRAMP 12	157	0.70	65	109

Histological Analysis

A block, containing the prostate was excised and further processed for histological analysis. It was cut through the urethra and 5 μm thick slices were evaluated. In the microscopic slides, the areas of the histologically homogenous regions, recognizable on the normalized R1 maps, were measured and their histological scores were determined. Noncancerous tissues were scored 1, 2, or 3, indicating healthy, low-grade PIN and high-grade PIN, respectively. Scores 4 indicated well-differentiated adenocarcinomas. Corresponding areas in the calculated R1, normalized R1, and Neoplastic Index maps

were also measured. For each region with a well-defined score, a fractional neoplastic area (neoplastic area/total prostate lobe area) was calculated both in the histological sections and in the R1 map. Other MRI related parameters (normalized R1, NI) measured in the corresponding regions were exported for further analysis.

Statistical Analysis

Statistical analysis of the data was carried out using SigmaStat version 2.03 (SPSS, Inc).

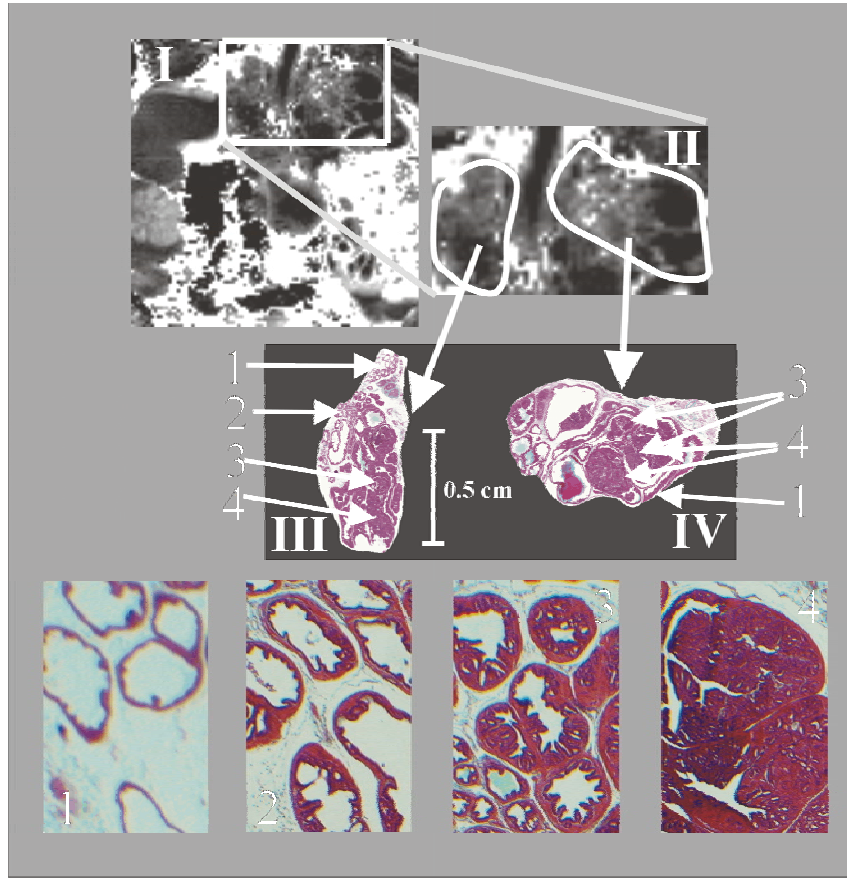


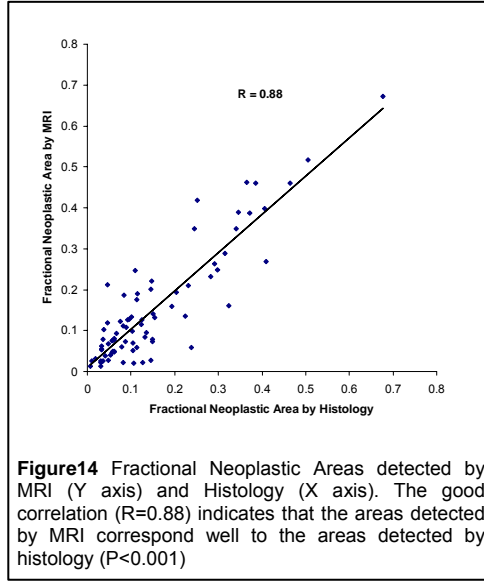
Figure13 The calculated R1 map (I), the magnified section of the prostate (II), and the histological sections of the two lobes (III-left lobe, IV-right lobe) are shown. Normal (score 1), low grade PIN (score 2), high grade PIN (score 3) and well differentiated adenocarcinoma (score 4) can be identified. The white arrows indicate the position of areas with different histological scores in the prostate tissue.

6.3 RESULTS

In Figure 13 the co-registration of the MRI delineated areas in the prostate lobes with the histological scores found in the corresponding physical prostate areas is shown. The

fractional neoplastic area values (see METHODS) obtained from the histological sections were correlated pairwise with values obtained from their corresponding R1 map (Fig. 14).

6.4 CONCLUSIONS



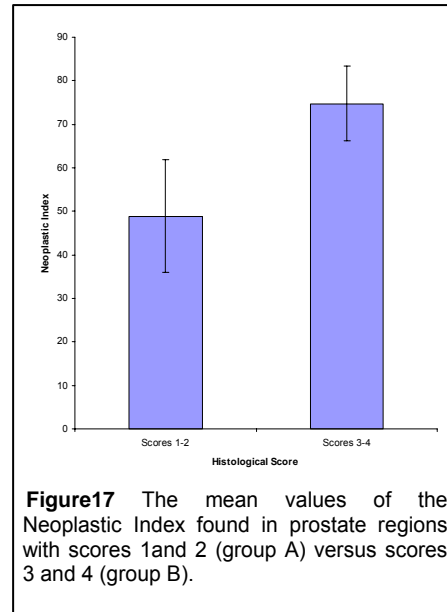
(score 4) within the murine prostate lobes. It is worth emphasizing that these lobes are often less than 5 mm in diameter, yet such tissue differentiation nevertheless has been possible with our technique. NI values (see METHODS Section) were also calculated pixel-by-pixel and were averaged in each prostate region. In Figure 17, the NI values measured in regions with different histological are shown.

As a conclusion, a non-invasive method, using R1 mapping in the presence of Gd(ABE- DTTA) could successfully be used to distinguish early phases of prostate neoplasm from its developed phases in TRAMP mice.

7 DISCUSSION

In our work we managed to prove that Gd(ABE-DTTA) can successfully be used at high field to measure R1 and so, create R1 maps. The relaxivity of Gd(DTPA), the most often used contrast agent in the clinic, decreases with increasing field strength. Gd(ABE-DTTA), on the other hand, demonstrates a local maximum in relaxivity at a very high

Our results indicate that Gd(ABE-DTTA) is distributed in the prostate in inverse proportion to the tissue's neoplastic content in the TRAMP mouse model. Thus, the R1 value of a given prostate volume element is governed by the fraction of neoplastic tissue of scores 3 and 4 in that volume element. Therefore, our results seem to show that an R1 map made following the administration of Gd(ABE-DTTA) can differentiate normal prostate tissue (score 1) or low score (score 2) mouse prostatic intraepithelial neoplasia(PIN) from tissues with either high score PIN (score 3) or well differentiated adenocarcinoma (WD)



field strength, around 5T (Fig. 2B). As our results demonstrate, this agent can be used at any field strength between 1.5 and 10T without significant loss of efficacy. In our myocardial ischemia canine experiments, based on the differential distribution of the CA in the ischemic vs. non-ischemic myocardium, the $\Delta R1_n$ values were significantly lower in the ischemic regions than in the non-ischemic areas during the ischemic period.

During reperfusion, this difference vanished (Fig. 4). In the individual experiments the lower $\Delta R1$ values showed regional correlation with the regional function parameters assessed by MRI (WT, WM), as well as with the MP values (Fig. 6). A good correspondence among the various maps is evident. The underperfused areas are clearly shown by the $\Delta R1_n$ map. Good correspondence is observed between the location of the underperfused sectors defined by the $\Delta R1_n$ map and that shown by the MP map, thus validating the former.

We have shown the extent to which the $\Delta R1_n$ values obtained after the injection of Gd(ABE-DTTA) reflect the myocardial perfusion. Once the correlation between MP and $\Delta R1_n$ has been established, a pixel-by-pixel $\Delta R1_n$ map can be translated into a PP map with the same resolution. It is worth mentioning that with this method the spatial resolution is higher than even in the post mortem gold standard set by the microsphere determination of MP, the resolution of which is about 1 cm³.

With using our contrast agent and method (R1 mapping) we studied a model of a completely different disease, prostate neoplasm in TRAMP mice, to see if they can be used in the diagnostics of such disease as well.

The post-contrast mean, normalized R1 obtained from regions with high-grade PIN & WD, however, are not different from the pre-contrast mean. This suggests that high-grade PIN and WD regions did not take up Gd(ABE-DTTA), contrary to the normal&low-grade PIN regions. A possible explanation, underlying our observations, may be an abnormal vasculature in the neoplastic prostate areas. Such prostate vasculature has been reported by Ozawa et al. Abnormal vasculature may reduce the access of the contrast agent to the high-grade PIN areas for the same reason that chemotherapeutic agents often fail to be taken up in tumors.

Our results are inconsistent with the findings in human studies where the post contrast MRI signal intensities were found to be higher in the cancerous areas than in the normal tissues. Our results can be well understood, however, in light of the studies by Jain et al. They have shown that in tumors during angiogenic development within a certain “time window”, the imbalance of the pro- and anti-angiogenic (thrombospondin-1 and VEGF, respectively) factors makes tissue blood circulation impaired due to formation of abnormal vasculature.

In summary, our method is equivalent to a post-mortem biopsy examining the entire prostate, yet done noninvasively. Therefore, our method yields an *in-vivo*-obtained virtual biopsy map (VBM).

In conclusion, in our work we have proven in models of multiple diseases that using a contrast agent with a sufficiently long half-life and with a preserved relaxivity in the high field, R1 map can provide more, quantitative and reproducible information to the clinicians.

8 NEW FINDINGS

8.1 A unique field dependency of Gd(ABE-DTTA) was found; unlike most of the commercially available MRI contrast agents, Gd(ABE-DTTA) showed a maximum relaxivity enhancement at around 5T. This makes it suitable for using it on high field. This is an important finding considering the recent trend of the MRI instruments' field strength.

8.2 Many of the imperfections of the SI based perfusion detection in the myocardium are mostly due to the single image method itself, such as field inhomogeneity, coil effects, etc. R1 measurements, however, can eliminate most of these effects. Presently, on most of the MRI instruments, the duration of an R1 measurement exceeds the half life of the commercially available contrast agents. Gd(ABE-DTTA) has a half life in the blood long enough to acquire such parameter in its present. It has successfully been used in a myocardial ischemia-reperfusion canine model to quantitatively and reproducibly detect myocardial ischemia on a voxel-by-voxel manner.

8.3 Most of the presently known MRI methods to detect human prostate neoplasm can only visualize prostate cancer in its developed phase. Using our contrast agent and the same method we successfully could detect TRAMP mouse prostate intraepithelial neoplasm in its early phase; we could distinguish mouse prostate voxels with mPIN score 1-2 from voxels with score 3 and above.

9 ACKNOWLEDGEMENTS

I wish to acknowledge the tremendous help of the following personnel:

Gabriel A Elgavish, PhD
Tamás Simor, MD, Ph.D.
Lajos Papp, MD, D.Sc.
Erzsébet Róth, MD, D.Sc.
Alexander Juhász-Nagy, MD, D.Sc. †
Ivan Horvath, MD, PhD,
Istvan Szokodi, MD, PhD
Miklos Tóth, MD, DSc
Pal Suranyi, MD, PhD
Balazs Ruzsics, MD, PhD
Attila Cziráki, MD, PhD
Isam A Eltoun, MD
Laszlo Hejjel, MD, PhD
Brandy Jewell
Violetta Kekesi, PhD
Attila Kovacs
Laszlo Lenard, MD, PhD
Eszter Szendrei
Huadong Zeng, PhD

I'm also thankful to my family for their tolerance.

10.1 PAPERS – RELATED TO THESIS

1. **P. Kiss**, P. Suranyi, T. Simor, N.H. Saab-Ismail, A. Elgavish, L. Hejjel, G.A. Elgavish: *In Vivo* R1-Enhancement Mapping of Canine Myocardium Using ceMRI with Gd(ABE-DTTA) in an Acute Ischemia-Reperfusion Model. *Journal of Magnetic Resonance Imaging; J Magn Reson Imaging*. 2006 Sep;24(3):571-9. **IF: 1.651**
2. B. Ruzsics, P. Surányi, **P. Kiss**, B.C. Brott, A. Elgavish, N.H. Saab-Ismail, G.A. Elgavish: Gd(ABE-DTTA), a novel contrast agent, at the MRI-effective dose shows absence of deleterious physiological effects in dogs. *Pharmacology*. 2006;77(4):188-94. *Epub* 2006 Jul 27. **IF:1.019**
3. P. Surányi, **P. Kiss**, T. Simor, A. Elgavish, G.A. Elgavish: A combined method for the determination of myocardial perfusion in experimental animals using microspheres and MRI. *Journal of Cardiovascular Magnetic Resonance*; 2007;9(3):549-56. **IF:2.016**
4. P. Suranyi, **P. Kiss**, B.C. Brott, T. Simor, A. Elgavish, B. Ruzsics, N.H. Saab-Ismail, G.A. Elgavish: Percent Infarct Mapping – A R₁-map Based ceMRI Method for Determining Myocardial Viability Distribution. *Magn Reson Med*. 2006 Sep;56(3):535-45. **IF: 3.405**
5. P. Suranyi, **P. Kiss**, B. Ruzsics, B.C. Brott, T. Simor, A. Elgavish, R.A. Baker, N.H. Saab-Ismail, G.A. Elgavish: In Vivo Myocardial Tissue Kinetics of Gd(ABE-DTTA), a Tissue-Persistent Contrast Agent. *Magn Reson Med*. 2007 Jul;58(1):55-64. **IF: 3.405**
6. P. Suranyi, **P. Kiss**, B. Ruzsics, B.C. Brott, T. Simor, G.A. Elgavish: Equilibrium Signal Intensity-Mapping, an MRI Method for Fast Mapping of Longitudinal Relaxation Rates and for Image Enhancement. *Magn Reson Imaging*. 2007 Jun;25(5):641-51. *Epub* 2006 Nov 21. **IF: 1.672**
7. B. Ruzsics, P. Surányi, **P. Kiss**, B. C. Brott, S. Litovsky, T.S. Denney Jr, I. Aban, S.G. Lloyd, T. Simor, G.A. Elgavish, H. Gupta: Myocardial strain in sub-acute peri-infarct myocardium. *Int J Cardiovasc Imaging*. 2009 Feb;25(2):151-9. **IF: 1.268**
8. B. Ruzsics, P. Surányi, **P. Kiss**, B. C. Brott, S.S. Singh, S. Litovsky, I. Aban, S.G. Lloyd, T. Simor, G.A. Elgavish, H. Gupta: Automated multidetector computed tomography evaluation of subacutely infarcted myocardium. *J Cardiovasc Comput Tomogr*. 2008 Jan;2(1):26-32. *Epub* 2007 Nov 19. **IF: not yet available**
9. B. Ruzsics, P. Surányi, **P. Kiss**, B. C. Brott, A. Elgavish, T. Simor, G.A. Elgavish: Head-to-head comparison between delayed enhancement and percent infarct mapping for assessment of myocardial infarct size in a canine model. *J Magn Reson Imaging*. 2008 Dec;28(6):1386-92. **IF: 1.651**

10. **P. Kiss**, I. A. Eltoun, P. Suranyi, H. Zeng, T. Simor, A. Elgavish, G. A. Elgavish: Virtual in vivo Biopsy Map of Early Prostate Neoplasm in TRAMP Mice by MRI. *Prostate*. 2009 Apr 1;69(5):449-58. **IF:2.601**

10.2 PAPERS – NOT RELATED TO THESIS

1. I. Szokodi, F. Horkay, B. Merkely, F. Solti, L. Geller, **P. Kiss**, L. Selmecci, V. Kekesi, O. Vuolteenaho, H. Ruskoaho, A. Juhasz-Nagy, M. Toth: Intrapericardial infusion of endothelin-1 induces ventricular arrhythmias in dogs. *Cardiovascular Research*. 38(2):356-64, 1998 May. 98375058 **IF: 3.092**

10.3 SUPPLEMENTS

1. F. Horkay, I. Szokodi, B. Merkely, F. Solti, L. Geller, **P. Kiss**, L. Selmecci, I. Horvath, V. Kekesi, A. Juhasz-Nagy, M. Toth: Potential pathophysiologic role of endothelin-1 in canine pericardial fluid. *Journal of Cardiovascular Pharmacology*. 31 Suppl 1:S401-2, 1998. 98257852 **IF: 1.709**

2. I. Szokodi, F. Horkay, **P. Kiss**, L. Selmecci, I. Horvath, O. Vuolteenaho, H. Ruskoaho, A. Juhasz-Nagy, M. Toth: Characterization of canine pericardial fluid endothelin-1 levels. *Journal of Cardiovascular Pharmacology*. 31 Suppl 1:S399-400, 1998. 98257851 **IF: 1.709**

3. P. Turbucz, **P. Kiss**, F. Horkay, I. Szokodi, R. deChatel, L. Selmecci, A. Juhasz-Nagy, I. Karadi, M. Toth: High pericardial fluid levels of endothelin are not caused by altered neutral endopeptidase activity in cardiac patients. *Journal of Cardiovascular Pharmacology*. 31 Suppl 1:S287-9, 1998. 98257817 **IF: 1.709**

4. **P. Kiss**, I. Horvath, I. Szokodi, P. Toth, V. Kekesi, A. Juhasz-Nagy, M. Toth: Endothelin does not interact with angiotensin II in the coronary vascular bed of anesthetized dogs. *Journal of Cardiovascular Pharmacology*. 31 Suppl 1:S103-5, 1998. 98257768 **IF: 1.709**

10.4 ORAL PRESENTATIONS

1. **P. Kiss**, P. Suranyi, T. Simor, N.H. Saab-Ismail, A. Elgavish, L. Hejjel, and G.A. Elgavish: In Vivo T1 Mapping of Canine Hearts Using Gd(ABE-DTTA) in an Ischemia-Reperfusion Model. *Oral presentation at the Annual Meeting of The International Society for Magnetic Resonance in Medicine, Toronto, ON, Canada, July 10-16, 2003*

2. **P. Kiss**, P. Surányi, B. Ruzsics, B.C. Brott, T. Simor, and G.A. Elgavish: Ex Vivo Percent Infarct Mapping Using Gd(DTPA): R1-Based MRI Quantification of Myocardial Viability. *Oral presentation at the 14th Annual Meeting of the North American Society for Cardiac Imaging 2006, Las Vegas, Nevada, USA*

10.5 POSTER PRESENTATIONS

1. **P. Kiss**, A. Gustin, D. Buchsbaum, T. Simor, L. Lenard, S. Vickers, and G.A. Elgavish ¹⁹F NMR As a Tool to Measure The Efficiency of Adenoviral CD Gene Transfer. In Vitro and In Vivo Monitoring of 5-FC to 5-FU Conversion. *Poster presentation at the Annual Meeting of The International Society for Magnetic Resonance in Medicine, Denver, CO, USA, April 1-7, 2000*
2. **P. Kiss**, L. Lenard, T. Simor, J. Forder, R. Mentor, A. Elgavish, and G.A. Elgavish MR Imaging As a Tool to Monitor Prostate Tumor Development in Mice with Mutant p53 Gene *Poster presentation at the Annual Meeting of The International Society for Magnetic Resonance in Medicine, Glasgow, Scotland, UK, April 21-27, 2001*
3. **P. Kiss**, T. Simor, L. Lenard, L. Hejjel, P. Suranyi, N.H. Saab-Ismail, and G. A. Elgavish Relaxivity of Gd(ABE-DTTA) Increases with Magnetic Field Strength Up to 5T. A Contrast Agent for High Field Imaging. *Poster presentation at the Annual Meeting of The International Society for Magnetic Resonance in Medicine, Honolulu, Hawaii, USA, May 18-26, 2002*
4. **P. Kiss**, A. Elgavish, I-E. Eltoum, P. Suranyi, H. Zeng, T. Simor, B. Ruzsics, G. A. Elgavish: Early Detection of Prostate Neoplasm Using Pixel-by-pixel R1 Mapping Following Gd(ABE-DTTA) Administration in TRAMP Mice. *Poster presentation at the 14th Annual Meeting & Scientific Sessions of International Society for Magnetic Resonance in Medicine, 2006, Seattle, Washington, USA.*

10.6 PATENT

G. A. Elgavish, P. Suranyi, T. Simor and **P. Kiss**: Differentiation of Tissue Clinical Parameters Using Nuclear Magnetic Resonance Techniques. Provisional Patent, U.S. Patent and Trademark Office No. 45,587. Docket Number **P72418US00GP**